International Journal of Nanoelectronics and Materials
Volume 13, No. 1, Jan 2020 [71-80]

Digital Fringe Projection System for Round Shaped Breast Tumor Detection

W. M. W. Norhaimi[1]*, Z. Sauli[1], H. Aris[1], V. Retnasamy[1], R. Vairavan[1] and M. H. A Aziz[1]

[1]*School of Microelectronic Engineering, Universiti Malaysia Perlis, Pauh Putra Campus, 02600 Arau, Perlis, Malaysia.*

Received 1 July 2019, Revised 6 September 2019, Accepted 7 October 2019

ABSTRACT

The digital fringe projection has been widely used in the field of surface imaging however its application in the field of body imaging especially for human breasts is still quite limited. Currently, the common imaging modality for breast tumor diagnoses are breast ultrasound and mammogram. There are advantages and limitations of using the mammogram and ultrasound in terms of the procedure of the process and the non-invasive nature of the procedure. In this work, an automated digital fringe projection system is developed to execute the imaging of surface changes of a helical shaped phantom breast. The fringe projection setup utilizes a computer, LCD projector, and a CCD camera. The tumor used was round-shaped with a diameter size of 1.5 and 2 cm. The fringe pattern was projected through the three-step phase shift where a resulting phase map was obtained. Results demonstrated that the system was able to identify an average pixel shift of five and ten on the breast surface caused by the presence of the round breast tumors.

Keywords: Breast Tumor, Breast Imaging, Digital Fringe Projection, Phase Shift.

1. INTRODUCTION

Early detection of breast cancer has been known to increase the survival rate of breast cancer patients. In the United States, breast cancer survival rates have increased from 75% in 1975-1977 to 90% in 2003-2009 [1]. The increase of breast cancer survival rates is due to the early diagnose of breast tumor screening and increasing awareness of breast cancer among women [2][3]. Some of the main factors that influence the survival rate of breast cancer patients are the tumor size and the number of axillary lymph nodes involved during the early stage of detection [4]. Early detection of breast cancer tumors may avoid cancer from metastasizing to other body organs. Since the primary focus of this work is on the tumor that causes changes to the surface of the breast, it is an important indicator to identify that the tumor size in the early stages of breast cancer is less than 2 cm [5].

Currently, the most common imaging modalities for breast tumor diagnose are mammography and breast ultrasound. The mammography which is known to apply a low dose of x-ray to observe within the breast has been known to provide false-positive (tumor is mistaken for being malignant) and false-negative (tumor mistaken for being benign) results after confirmation with biopsy [6]. One of the main causes for these differing results was due to the density of the breast. The breast ultrasound, on the other hand, is another option for breast cancer screening for the dense breast. The advantage of breast ultrasound is that it is radiation-free and more tolerable for patients.

*Corresponding Author: *wanmokhdzani@unimap.edu.my*

Although the breast ultrasound is more sensitive towards the dense breast, the image interpretation of the ultrasound highly depends on the expertise of the radiologist. Another imaging modality that has been frequently used is the Computer-Aided Diagnose (CAD). The CAD imaging requires the images from a mammogram or ultrasound for the image processing, image segmentation, feature extraction, and classification. CAD system has been highly known to assist the radiologist in classifying tumors [7].

The imaging modality to be applied in this work is a digital fringe projection system and is used to identify surface changes of a breast due to the presence of tumors [8]. The digital fringe projection utilizes the phase-shifting concept mainly comprising of a computer, light projection and image capturing. The digital fringe projection has been previously applied in various applications namely 3D surface shape and deformation measurement [9][10], surface profiles of electronic and semiconductor industry [11] and old sophisticated artifact objects [12]. In the field of human body imaging, the digital fringe projection has been known to provide a worthy 3D topography of the human body [13]. In-vivo various human skin type has also been imaged using fringe projection although test subjects of patients with skin cancer have not been tested [14]. The images captured from the fringe projection has also been used to identify the postural formation of boys and girls and their tendency to develop into structural scoliosis [15][16]. The application of digital fringe projection on the human body has been proven to be applicable in identifying certain diseases that correspond with external structure changes of the human body. Digital fringe projection is also a non-invasive method where the only light is used as the source of imaging rather than the use of x-rays or gamma rays. Therefore, the digital fringe projection to be applied in this work will identify the surface changes of a phantom helical breast caused by the presence of round shaped tumors. Round shaped tumors with a diameter of 1.5 and 2 cm are used as tumors since tumor size during stage 1 and 2 are less than 2 cm [5]. The fringe projection will be based on fringe phase shifting and pixel coordinate tracking.

2. RESEARCH METHODOLOGY

The research methodology consists of three main components of the digital fringe projection system which are the digital fringe projection setup, fringe pattern development and fringe calibration based on fringe visibility.

2.1 Digital Fringe Projection Setup

The digital fringe projection setup that was developed is based on the phase-shifting technique. The setup mainly comprises of a computer, LCD projector (Panasonic PTLW80NTEA) and a 1392 x 1040 resolution CCD camera (AVT Marlin F-146C), as shown in Figure 1. The projector was used as the source of structured light while the CCD camera was used as a means of capturing the projected fringe. Both the projector and the camera communicate with the same computer. The projection angle of the projector was also set to not exceed 45 degrees to avoid shadows from the projection and to obtain uniform illumination on the test reference setup [17]. The processing of a fringe pattern is executed using the UU image processing software [18]. The tumor was inserted into the helical breast sample through an automated insertion mechanism using Arduino microcontrollers with a servo motor gear mechanism. The servo motor movement was programmed to rotate a gear that was connected to the tumor sample thus enabling it to move in a bidirectional vertical axis.

The fabrication of breast tumors has been extensively constructed by some researchers during the last decade. Most of the researchers mainly applied a mixture of water, oil, and gelatin [19][20]. The tumor sample fabricated in this work comprised of a mixture of oil, water, and flour with a ratio of 10:40:50. The mixture was stirred in a beaker for 10 minutes. Once the mixture began to slightly harden, round-shaped tumor samples were then formed with a

diameter of 1.5 and 2 cm. Once a tumor has been fabricated, the tumor sample must be immediately inserted into the phantom helical breast for fringe image capturing in order to avoid the tumor becoming too hard thus reducing its elasticity characteristics.

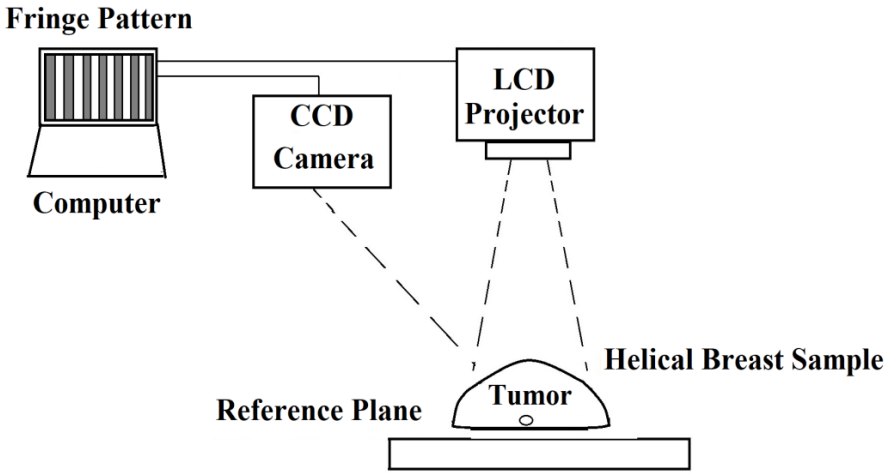

Figure 1. Digital fringe projection setup comprising of the CCD camera, helical breast sample, LCD projector and fringe patterns generated through the computer.

2.2 Fringe Pattern Development

The fringe pattern was developed using the C++ language and was applied to generate three fringe patterns with different phases. The phase is shifted every 2π/3 radians respectively for the three different fringe patterns. Since phase shifting is executed based on computer-generated fringe patterns, phase shifting becomes more accurate and no physical device is involved for the phase shifting process. The three fringe patterns of different phases were then projected onto the helical shaped breast with the presence of the phantom tumor within the breast. The mathematical descriptions of these three fringe patterns are shown in Equation (1), (2) and (3) [8]:

$$I_1 = A(i,j) + B(i,j)\cos\phi(i,j) \quad (1)$$

$$I_2 = A(i,j) + B(i,j)\cos[\phi(i,j) + \frac{2\pi}{3}] \quad (2)$$

$$I_3 = A(i,j) + B(i,j)\cos[\phi(i,j) + \frac{4\pi}{3}] \quad (3)$$

where: I_1, I_2, I_3 : Recorded Intensity of fringe pattern
$A(i,j)$: Uniform background intensity
$B(i,j)$: Amplitude of sinusoidal waveform
$\varphi(i,j)$: Phase angle at point (i,j)

Phase mapping is then executed based on the three-step phase-shifting algorithm by evaluating $\phi(i,j)$ simultaneously with Equation (1), (2) and (3) which leads to Equation (4):

$$\phi(i,j) = \tan^{-1}[\frac{\sqrt{3}[I_3(i,j) - I_2(i,j)]}{2I_1(i,j) - I_2(i,j) - I_3(i,j)}] \quad (4)$$

2.3 Fringe Pattern Calibration based on Fringe Visibility

Once the fringe projection system has been set up with the fringe projection, calibration has to be done in order to optimize the accuracy of fringe images for pixel location analysis of the

helical phantom breast. The calibration of the setup involves the camera alignment and its aperture where fringe contrast is used. Fringe contrast of the setup is essential to reduce errors of the pixel tracing from the fringe image [21]. Once a projector has been aligned with the reference plane, the CCD camera's aperture was experimented to obtain higher Fringe Visibility (FV) in order to achieve higher fringe contrast. FV was obtained as in Equation (5). The aperture of the CCD camera used was f/1.4, f/2, f/2.8, f/4, f/5.6, f/8, f/11 and f/16.

$$FV = \frac{I_{\max} - I_{\min}}{I_{\max} + I_{\min}} \tag{5}$$

where: I_{max} : Maximum intensity of the bright fringe
I_{min} : Minimum intensity of the dark fringe

The FV from the varied apertures of the CCD camera is tabulated in Table 1. The maximum possible intensity to be obtained is a grayscale value of 255 while the minimum possible value for the dark fringe is a phase value of 0 which corresponds with the range [–π, +π]. Other phase values are linearly associated with the pixel intensity from 0 to 255. Based on the intensity of the bright (I_{max}) and dark (I_{min}) fringe obtained from the different aperture, it can be clearly seen that the aperture size of f/5.6 has the highest intensity and a relatively low dark fringe intensity thus providing fringe visibility of 0.81. A lower aperture value provides a wider aperture size which results in a shallow depth of field thus contributing to the small difference of intensity between the bright and dark fringe as demonstrated by the fringe visibility obtained from aperture size f/1.4 – f/4. Aperture size ranging from f/5.6 – f/16 provides a deeper depth of field, therefore, creating a contrast between the bright and dark fringe. Based on the fringe visibility obtained from the different aperture size, an aperture size of f/5.6 is selected for the fringe projection as shown in Figure 2.

Table 1 Fringe visibility of fringe patterns at different camera apertures

Aperture	Imax	Imin	FV
f/1.4	255.00	237.68	0.04
f/2	255.00	224.36	0.06
f/2.8	255.00	227.64	0.06
f/4	255.00	99.71	0.44
f/5.6	255.00	26.86	0.81
f/8	200.00	45.00	0.63
f/11	140.00	27.14	0.68
f/16	55.00	15.00	0.57

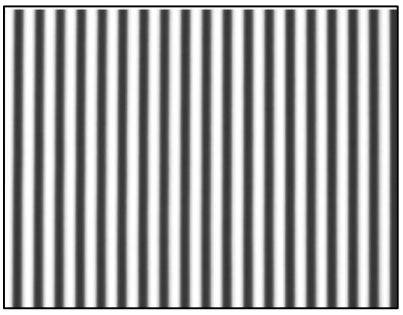

Figure 2. Fringe pattern visibility for aperture f/5.6.

3. RESULTS AND DISCUSSION

3.1 Processing of Fringe Pattern Analysis

The three fringe patterns generated by C++ coding was shifted by 2π/3 radians on the computer and projected onto the surface of the helical phantom breast. The 2π/3 radians phase shift was selected due to its suitability in obtaining phase map image without noise distortion. The 2π/3 phase shift is commonly adopted in the three-step phase shift fringe projection compared to the π/2 phase shift of four-step fringe projection due to the least amount of measurement time required [22] [23] [24]. Each of the three shifted fringe patterns image were recorded with the CCD camera. The phase mapping algorithm was applied to the three recorded images to obtain the wrapped phase image as shown in Figure 3.

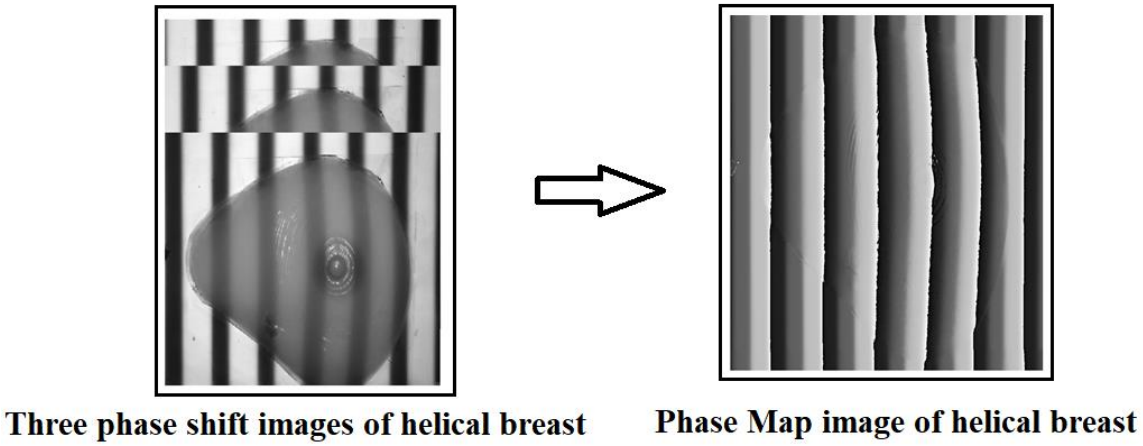

Figure 3. Phase map image of the helical shaped breast obtained from the phase-shifting process.

Once the phase map image was obtained, pixel coordinates of the helical shaped breast without tumor were mapped with digital markers as illustrated in Figure 4. A total of 156 digital markers were used with a distance of 80 pixels separating them. The location of the digital markers covered the entire helical breast surface area.

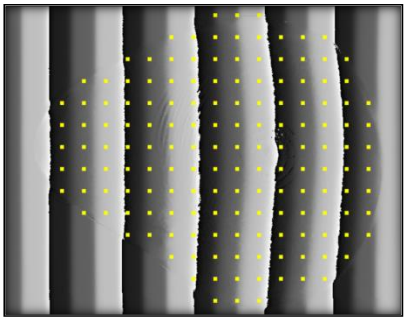

Figure 4. Phase map image of the helical shaped breast obtained from the phase-shifting process.

The 1.5 and 2 cm tumors were then inserted into the phantom breast where a surface variation of the breast occurs thus enabling the pixel coordinate tracking to be executed. The grayscale values obtained from the wrapped phase image of both tumors were determined for pixel tracking. Values of the grayscale value range from 0 - 255 correspondings with the fringe width. Comparisons were then made between the grayscale values of the different tumor sizes with the reference helical phantom breast. If a variation of grayscale value is found on each of the breast surfaces with the tumors, pixel tracing was then executed and compared to the initial breast

surface to determine the equal grayscale value. Once the grayscale value has been traced, the new coordinate point will then be used to determine the changes of the helical breast surface caused by the presence of the tumors.

3.2 Pixel Coordinate Tracking from Fringe Analysis

Based on the digital markers which were marked on the phase map image of the reference breast sample and breast tumor samples, a variation of grayscale value can be observed. The variation of the grayscale value caused by the presence of 1.5 and 2 cm tumor is shown in Figure 5. The blue line is the coordinate mapping of the helical breast without the presence of a tumor while the red dash line is coordinate mapping of the helical breast with the presence of a 1.5 cm tumor. The green dotted line illustrates the mapping of the helical breast with the presence of a 2 cm tumor. The shifting of pixel location is evident for the 1.5 cm tumor at x-axis 970 and 1050 where the pixel coordinates shift with an average of five pixels from the reference coordinates. It can be clearly seen that the other digital coordinate markers overlap with each other indicating that the tumor only causes a pixel change at the location of breast insertion.

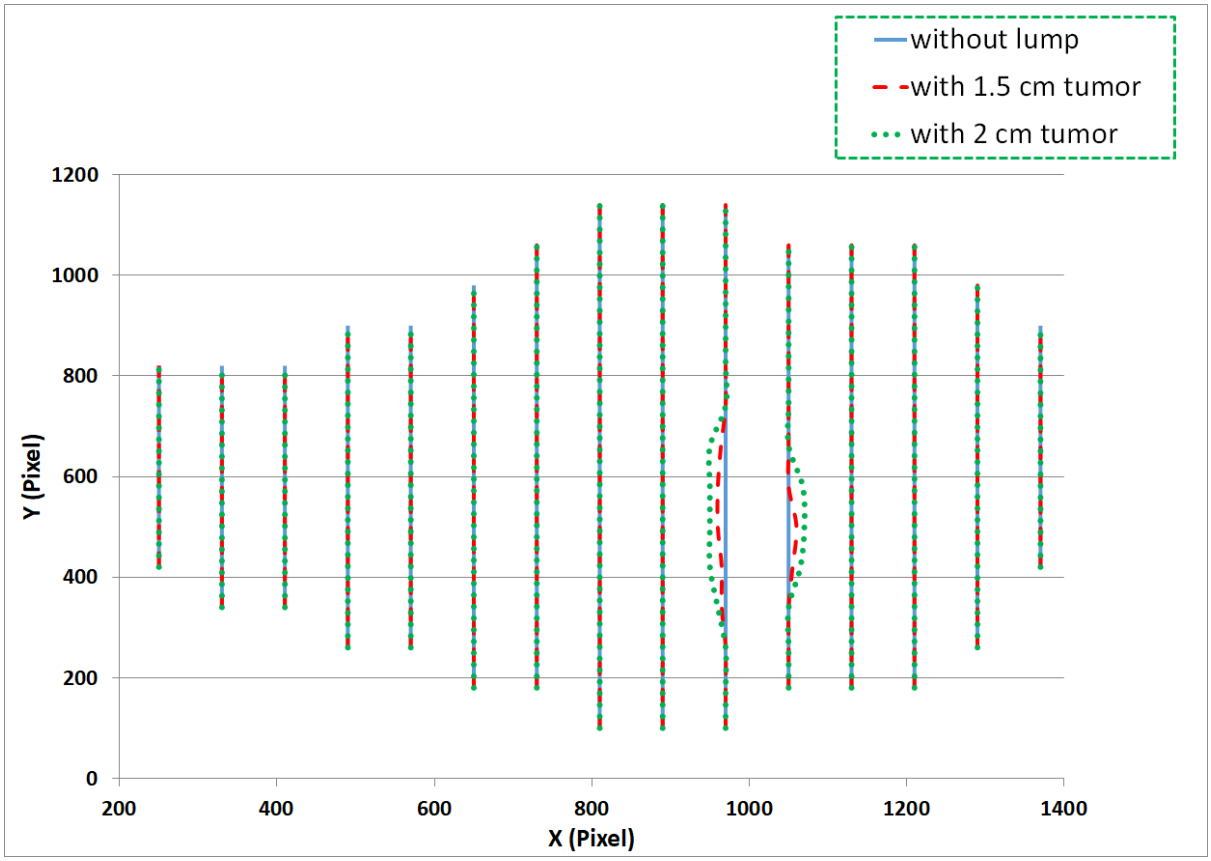

Figure 5. Pixel coordinate mapping of 1.5 and 2 cm round-shaped breast tumor markers for phase map image of a helical breast.

The presence of a tumor was also detected at the x-axis of 970 and 1050 for the 2 cm tumor. However, the pixel coordinate shift is slightly larger than the 1.5 cm tumor where the pixel shift is roughly 10 from the reference map as shown in Figure 6. The major pixel shift at 970 and 1050 axis are caused by the location of tumor insertion which is placed at the chest cavity of the helical breast just below the breast nipple area.

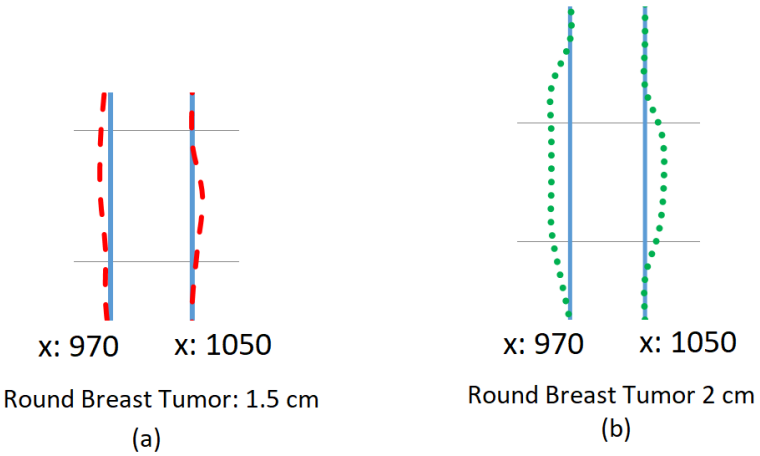

Figure 6. Pixel shift comparison of 1.5 and 2 cm at x-axis 970 and 1050.

The round tumor size of 2 cm clearly causes a larger pixel location shift compared to a tumor size of 1.5 cm due to the larger tumor size. The results obtained from the pixel shift caused by the tumors are also similar to previous results obtained from a similar helical phantom breast [8]. The difference from their work was based on the larger pixel shift obtained caused by using a metal screw as their tumor. Screws are stiff and cause a larger displacement to the breast surface. The force of the circular and round tumor causes changes to the surrounding breast tissue thus causing a surface change of the helical breast. This is also due to the elastic and stiff nature of the tumor compared to normal breast tissue [25]. Both benign and malignant tumors are significantly stiff and elastic which causes a displacement within the breast. Malignant tumor with a size of 1.5 and 2 cm are within the borders of a stage 2 breast carcinoma. This will possibly enable the digital fringe projection system to detect possible early symptoms of breast cancer.

4. CONCLUSION

The digital fringe projection system employed in this work has demonstrated its capability in identifying surface breast changes caused by the presence of tumor size of 1.5 cm and 2 cm. The system which employs fringe phase shifting and pixel coordinate tracing was able to distinguish the displacement occurring on the breast surface caused by the round-shaped breast tumors. This implies that the digital fringe projection system can also be applied as a non-invasive imaging modality for breast cancer screening. A possible improvement to the fringe projection system will be to employ smaller tumor sizes to optimize its capability in detecting smaller round shaped tumors. Although the developed fringe projection setup was able to determine surface changes of the helical breast, the further test still needs to be done on in vivo patients who are known to have early stages of breast tumor progression.

ACKNOWLEDGMENTS

This work was supported financially by the Ministry of Higher Education of Malaysia (MOHE), Malaysia. Supporting aid from the School of Microelectronic Engineering, Universiti Malaysia Perlis was highly appreciated.

REFERENCES

[1] Siegel, R., DeSantis, C., Virgo, K., Stein, K., Mariotto, A., Smith, T., Cooper, D., Gansler, T., Lerro, C., Fedewa, S. & Lin, C., "Cancer treatment and survivorship statistics," CA. Cancer J. Clin. **62**, 4 (2012) 220–241.

[2] Berry, D. A., Cronin, K. A., Plevritis, S. K., Fryback, D. G., Clarke, L., Zelen, M., Mandelblatt, J. S., Yakovlev, A. Y., Habbema, J. D. F. & Feuer, E. J., "Effect of screening and adjuvant therapy on mortality from breast cancer: Commentary," Obstetrical and Gynecological Survey **61**, 3. (2006) 179–180.

[3] R. De Gelder, E. A. M. Heijnsdijk, J. Fracheboud, G. Draisma & H. J. De Koning, "The effects of population-based mammography screening starting between age 40 and 50 in the presence of adjuvant systemic therapy," Int. J. Cancer **137**, 1 (2015) 165–172.

[4] S. Saadatmand, R. Bretveld, S. Siesling & M. M. A. Tilanus-Linthorst, "Influence of tumour stage at breast cancer detection on survival in modern times: Population based study in 173 797 patients," BMJ **351** (2015) h4901.

[5] H. G. Welch, P. C. Prorok, A. J. O'Malley & B. S. Kramer, "Breast-Cancer Tumor Size, Overdiagnosis, and Mammography Screening Effectiveness," N. Engl. J. Med. **375**, 15, (2016) 1438–1447.

[6] A. Jalalian, S. B. T. Mashohor, H. R. Mahmud, M. I. B. Saripan, A. R. B. Ramli & B. Karasfi, "Computer-aided detection/diagnosis of breast cancer in mammography and ultrasound: A review," Clinical Imaging **37**, 3. Elsevier, (2013) 420–426.

[7] Y. S. Huang, E. Takada, S. Konno, C. S. Huang, M. H. Kuo & R. F. Chang, "Computer-Aided tumor diagnosis in 3-D breast elastography," Comput. Methods Programs Biomed. **153**, (2018) 201–209.

[8] Vairavan, R., Ong, N. R., Sauli, Z., Shahimin, M. M., Kirtsaeng, S., Sakuntasathien, S., Alcain, J.B., Paitong, P. & Retnasamy, V., "Fringe projection application for surface variation analysis on helical shaped silicon breast," in AIP Conference Proceedings **1885**, 1 (2017) 20251.

[9] U. Paul Kumar, U. Somasundaram, M. P. Kothiyal & N. Krishna Mohan, "Single frame digital fringe projection profilometry for 3-D surface shape measurement," Optik (Stuttg). **124**, 2, (2013) 166–169.

[10] H. Shi, H. Ji, G. Yang & X. He, "Shape and deformation measurement system by combining fringe projection and digital image correlation," Opt. Lasers Eng. **51**, 1 (2013) 47–53.

[11] F. Deng, Y. Ding, K. Peng, J. Xi, Y. Yin & Z. Zhu, "Three-dimensional surface inspection for semiconductor components with fringe projection profilometry," In Optical Metrology and Inspection for Industrial Applications IV. International Society for Optics and Photonics **10023**, 100230Y (2016).

[12] Z. Zhang, "Robust color and shape measurement of full color artifacts by RGB fringe projection," Opt. Eng. **51**, 2, (2012) 21109.

[13] Ares, M., Royo, S., Vidal, J., Campderrós, L., Panyella, D., Pérez, F., Vera, S. & Ballester, M.A.G., "3D scanning system for in-vivo imaging of human body," in Fringe 2013 - 7th International Workshop on Advanced Optical Imaging and Metrology (2014) 899–902.

[14] M. Ares, S. Royo, M. Vilaseca, J. A. Herrera, X. Delpueyo & F. Sanabria, "Handheld 3D Scanning System for In-Vivo Imaging of Skin Cancer," in upcommons.upc.edu (2014) 231–236.

[15] R. M. C. Aroeira, E. B. de Las Casas, A. E. M. Pertence, M. Greco & J. M. R. S. Tavares, "Non-invasive methods of computer vision in the posture evaluation of adolescent idiopathic scoliosis," Journal of Bodywork and Movement Therapies **20,** 4 (2016) 832–843.

[16] V. N. Sarnadskiy, "The structure of postural disorders and spinal deformities in age and gender according to computer optical topography," in Studies in Health Technology and Informatics **176** (2012) 77–82.

[17] L. Chen and C. Quan, "Reply to Comment on 'Fringe projection profilometry with nonparallel illumination: a least-squares approach,'" Opt. Lett. **31**, 13, (2006) 1974.

[18] L. Chen, "An image-processing software package: UU and Fig for optical metrology applications," in International Conference on Optics in Precision Engineering and Nanotechnology (icOPEN2013), **8769**, (2013) 87690U.

[19] S. Alshehri, A. Jantan, R. S. A. Raja Abdullah, R. Mahmud, S. Khatun & Z. Awang, "A UWB imaging system to detect early breast cancer in heterogeneous breast phantom," in InECCE 2011 - International Conference on Electrical, Control and Computer Engineering, (2011) 238–242.

[20] B. Ustbas, D. Kilic, A. Bozkurt, M. E. Aribal & O. Akbulut, "Silicone-based composite materials simulate breast tissue to be used as ultrasonography training phantoms," Ultrasonics **88** (2018) 9–15.

[21] Mao, J., Yin, Y., Meng, X., Yang, X., Lu, L., Li, D., Pape, C. & Reithmeier, E., "Two-step phase shifting in fringe projection: modeling and analysis," In Optical Micro-and Nanometrology VII (Vol. 10678, p. 106780V). International Society for Optics and Photonics, (2018) 32.

[22] C. Zuo, S. Feng, L. Huang, T. Tao, W. Yin & Q. Chen, "Phase shifting algorithms for fringe projection profilometry: A review," Optics and Lasers in Engineering, **109**, Elsevier, (2018) 23–59.

[23] G. Fu, Y. Cao, Y. Wang, Y. Wan, L. Wang & C. Li, "Real-time three-dimensional shape measurement based on color binary fringe projection," Opt. Eng. **58**, 4 (2019) 1.

[24] Feng, S., Zuo, C., Tao, T., Hu, Y., Zhang, M., Chen, Q. & Gu, G., "Robust dynamic 3-D measurements with motion-compensated phase-shifting profilometry," Opt. Lasers Eng., **103** (2018) 127–138.

[25] W. K. Moon, R.-F. Chang, C.-J. Chen, D.-R. Chen & W.-L. Chen, "Solid Breast Masses: Classification with Computer-aided Analysis of Continuous US Images Obtained with Probe Compression," Radiology **236,** 2 (2007) 458–464.